Received: 15 November 2018 | Revised: 1 March 2019 | Accepted: 19 March 2019

DOI: 10.1002/asl.898

RESEARCH ARTICLE

Atmospheric Science Letters RMetS

Seasonal prediction of equatorial Atlantic sea surface temperature using simple initialization and bias correction techniques

Tina Dippe[1] | **Richard J. Greatbatch**[1,2] | **Hui Ding**[3]

[1]Ozeanzirkulation und Klimadynamik, GEOMAR Helmholtz Centre for Ocean Research Kiel, Kiel, Germany

[2]Faculty of Mathematics and Natural Sciences, Christian Albrechts Universität, Kiel, Germany

[3]Cooperate Institute for Research in Environmental Sciences – University of Colorado and NOAA Earth Systems Research Laboratory, Boulder, Colorado

Correspondence
Richard J. Greatbatch, FB1/TM, GEOMAR Helmholtz Center for Ocean Research Kiel, Wischhofstr 1-3, 24105 Kiel, Germany.
Email: rgreatbatch@geomar.de

Funding information
PREFACE, Grant/Award Number: 603521; The European Union 7th Framework Programme, Grant/Award Number: FP7 2007–2013; German Ministry for Education and Research (BMBF)

Due to strong mean state-biases most coupled models are unable to simulate equatorial Atlantic variability. Here, we use the Kiel Climate Model to assess the impact of bias reduction on the seasonal prediction of equatorial Atlantic sea surface temperature (SST). We compare a standard experiment (STD) with an experiment that employs surface heat flux correction to reduce the SST bias (FLX) and, in addition, apply a correction for initial errors in SST. Initial conditions for both experiments are generated in partially coupled mode, and seasonal hindcasts are initialized at the beginning of February, May, August and November for 1981–2012. Surface heat flux correction generally improves hindcast skill. Hindcasts initialized in February have the least skill, even though the model bias is not particularly strong at that time of year. In contrast, hindcasts initialized in May achieve the highest skill. We argue this is because of the emergence of a closed Bjerknes feedback loop in boreal summer in FLX that is a feature of observations but is missing in STD.

KEYWORDS
Atlantic Niño, Atlantic warm bias, seasonal prediction

1 | INTRODUCTION

The Atlantic Niño is the dominant mode of interannual variability in tropical Atlantic sea surface temperatures (SST) (Zebiak, 1993; Xie and Carton, 2004). It is closely related to the seasonal cycle (Keenlyside and Latif, 2007; Ding *et al.,* 2009; Burls *et al.,* 2011; 2012), which in turn is dominated by the formation of the cold tongue in boreal summer. Cold tongue growth and decay are not symmetrical. Cooling between April and August is enhanced relative to the more gradual warming between August and March (cf. Figure 1). Burls *et al*. (2011) suggest that the reason for this is a seasonally active Bjerknes feedback (Bjerknes, 1969).

The Atlantic Niño is a modulation of the cold tongue development. While the name 'Atlantic Niño' suggests a phenomenon that is an Atlantic version of the Pacific El Niño-Southern Oscillation (ENSO), a number of important distinctions exist (e.g., Keenlyside and Latif, 2007). In particular, total SST variability in the tropical Pacific is established to similar degrees by the seasonal cycle and interannual variability (e.g., Burls *et al.,* 2011), whereas in the tropical Atlantic, it is clearly dominated by the seasonal cycle. Also, while ENSO is phase-locked to boreal winter, the Atlantic Niño peaks in May–July and is a modulation of the annual growth of the cold tongue and has much smaller amplitude than ENSO. While the growth of both Atlantic and Pacific Niño events is supported by the Bjerknes

Tina Dippe and Richard J. Greatbatch contributed equally to this study.

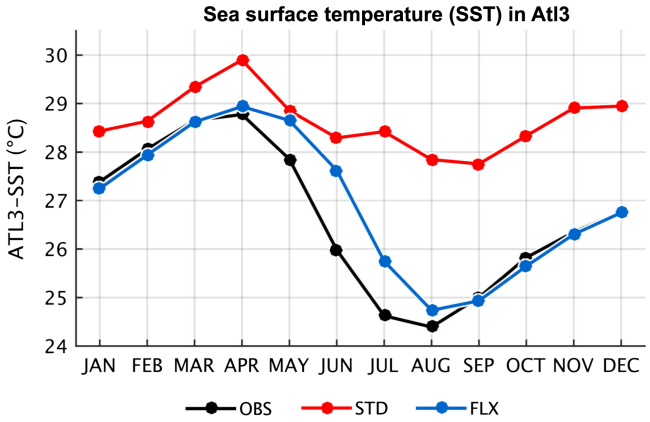

FIGURE 1 Monthly mean SST in (black) ERA-Interim and the (blue) FLX and (red) STD initialization runs in the Atl3 region ([−3,3]° N and [−20,0]°E)

feedback, the Atlantic Niño is more damped than ENSO (Lübbecke and McPhaden, 2013) and the associated atmosphere–ocean coupling is weaker (Dippe *et al*., 2019).

Irrespective of its dynamics, the Atlantic Niño is a mode of equatorial SST variability that produces teleconnections (Mohino and Losada, 2015). Via its relationship with the intertropical convergence zone, it affects rainfall variability over the surrounding continents, impacting their socio-economics (Hirst and Hastenrath, 1983). This motivates efforts to forecast Atlantic Niño events.

Current-generation coupled global climate models (CGCMs) struggle to simulate the Atlantic Niño. The reason is that almost all CGCMs suffer from a severe, seasonally varying bias in the equatorial-to-subtropical eastern South Atlantic (e.g., Stockdale *et al.,* 2006; 2011; Richter and Xie, 2008; Grodsky *et al.,* 2012; Wang *et al.,* 2014; Dippe *et al.,* 2018b). The bias is reflected in the SST field, its annual mean pattern stretching from the Angolan and Namibian coast into the ATL3 region ([−3,3]°N and [−20,0]°E). On the equator, the SST bias can reverse the sign of the SST gradient compared to observations. This reversal is complemented by a flattening thermocline (see Figure S1 in Ding *et al.,* 2015) that shoals slightly in the west and deepens in the eastern ocean basin.

It is well known that tropical Atlantic SST is particularly difficult to predict (Stockdale *et al.,* 2006; 2011). Here, we address the question: Does the SST bias affect the predictability of SST variability in the equatorial Atlantic? The study is based on earlier findings by Ding *et al*. (2015) and Dippe *et al*. (2018a) who showed that a simple bias alleviation technique strongly reduces the SST bias of a CGCM and improves the simulated SST variability for most of the year. The rest of the paper is structured as follows. Section 2 introduces our model, experimental set-up, initialization technique and bias reduction method. Section 3 presents the effect of the bias reduction on the initialization runs and assesses its impact on the predictive skill of SST in hindcast simulations. A summary and discussion is provided in Section 4. In the Supporting Information, we repeat our analysis for the tropical Pacific and compare it with the predictive skill in the tropical Atlantic.

2 | MODEL AND METHODS

Validation of model results in this study is based on the ERA-Interim reanalysis dataset (Dee *et al.,* 2011) for the period 1981–2012. While we are aware that a reanalysis is not identical with observations, we assume for this study that ERA-Interim is 'the truth'. The data can be accessed at the European Centre for Medium-Range Weather Forecasts (ECMWF: http://www.ecmwf.int/en/research/climate-reanalysis/era-interim). When we repeat our analysis with different SST datasets, we find that qualitative differences in the results are negligible.

Model runs were performed with the Kiel Climate Model (KCM, Park *et al.,* 2009). The KCM is a CGCM that consists of the atmospheric general circulation model ECHAM5 (Roeckner *et al.,* 2003) and the Nucleus of European Modeling of the Ocean (NEMO, Madec *et al.,* 1998; 2008) ocean–sea ice general circulation model. The coupler is the Ocean Atmosphere Sea Ice Soil version 3 (OASIS3, Valcke, 2013). For our experiments, we used a low-resolution version of the KCM: ECHAM5 is run in T31 horizontal resolution with 19 vertical levels and NEMO in the ORCA2-setup, which employs a horizontal resolution of roughly 2° in latitude and longitude, refined to 0.5° in latitude close to the equator and 31 vertical levels.

We base our results on two experiments. The first experiment uses a standard version of the KCM (STD). The STD-SST climatology contains the SST bias in the tropical Atlantic, which is comparable to the corresponding bias in other low-resolution CGCMs (Davey *et al.,* 2002; Richter and Xie, 2008). The second set of experiments employs surface heat flux correction to reduce the SST bias (FLX, see below). For both experiments, we produced a partially coupled set of initialization runs, which provides the initial conditions for our fully coupled hindcasts. It should be noted that radiative forcing varies only seasonally in this version of KCM.

Partial coupling has shown some success for initializing decadal hindcasts (Ding *et al.,* 2013; Thoma *et al.,* 2015). Bell *et al*. (2004) showed that assimilation of thermal data on the equator can lead to spurious vertical ocean circulation that triggers an initialization shock in the hindcasts. The reason is that the assimilation of thermal data disrupts the balance between zonal wind stress and the ocean zonal pressure gradient. Partial coupling avoids this problem by forcing the ocean and sea ice components of the coupled model with

observed wind stress anomalies that are added to the model's wind stress climatology without any additional data assimilation. This set-up retains thermal coupling between the atmosphere and the ocean and preserves SST and the atmospheric wind field as fully prognostic variables. In our experiments, we use monthly mean wind stress anomalies from ERA-Interim. The model wind stress climatology is diagnosed from a long control experiment of the KCM. Note that the STD and FLX experiments require separate control runs because their wind stress climatologies are not identical. We run three ensemble members, differing only in their initial conditions, for each of the STD and FLX initialization runs.

Surface heat flux correction is employed in the FLX-experiments to reduce the SST bias of the KCM. To diagnose the heat flux correction term, we use a long control run of the KCM during which we nudge the model towards the observed SST monthly mean seasonal cycle with a time scale of 10 days. After 470 years, when the model climate has stabilized, we use the following 70 years of the integration to diagnose the monthly mean heat flux that is associated with the SST restoring term. This is the heat flux correction climatology that we add noninteractively to our SST equation when running the KCM in heat-flux corrected mode.

The initialization runs for both experiments are produced in partially coupled mode with the respective version of the KCM (i.e., standard for STD and heat flux corrected for FLX). From the initialization runs, we start the fully coupled hindcasts (historical forecasts). Each hindcast consists of nine ensemble members and runs for 6 months. Hindcasts start on the first of February, May, August and November, for each year from 1981 to 2012. A suite of different initial conditions for the individual hindcast ensemble members is generated by mixing the atmospheric and oceanic states of the initialization run ensemble members, producing sets of nine different initial conditions for our hindcasts. Despite the simplicity of our method, Scaife *et al*. (2019) show that the hindcast skill for tropical rainfall in the STD experiments is comparable to that of much more sophisticated forecast systems that use full field initialization. This gives us confidence that useful insights can be gained from our experiments.

Finally, an integral measure of both forecast skill and the ability of the initialization run's ensemble mean to capture observed variability is the anomaly correlation coefficient (ACC) between the model simulations and the validation dataset (ERA-Interim). The reference for our monthly anomalies is the linear fit. The linear fit is a linear function that uses the slope and intercept parameters of least-squares fitting of the data. It corresponds to the evolution of the time series when only the linear trend is considered. Based on the linear fit, we calculate anomalies for the ACC as follows. (a) For each continuous *initialization run and for ERA-Interim*, we subtract, for each calendar month, the linear fit from the full data. The analysis period is 1981–2012. For the initialization runs, we calculate the linear fits and hence the anomalies separately for each ensemble member. The ensemble mean monthly anomaly is the average of the monthly anomalies of all ensemble members. (b) For the 6-months-long *hindcasts*, we stratify the data into ensemble members and months, where all ensemble members with the same label are based on the same combination of initial conditions. For each ensemble member, we select a given lead month and concatenate the data into a time series for that month. Based on these time series, we compute the linear fit for the hindcast data for each lead month and each ensemble member separately. Monthly anomalies and the ensemble mean anomaly are then calculated as before.

3 | RESULTS

3.1 | Initialization runs: initial conditions for the hindcasts

Figure 1 shows the seasonal cycle of ATL3 SST for the observations and the two initialization runs. The observed seasonal cycle shows strong initial cooling in April–May. Cooling decreases in June and stops in August, when the cold tongue starts to dissipate. The STD experiment is heavily biased with respect to the observations throughout the entire year. While the bias is moderate in boreal winter, it rapidly intensifies from June onwards. Mean bias values are 2.00°C and 3.08°C in the annual mean and for June–September, respectively. Heat flux correction reduces the annual mean bias to 0.29°C. FLX-SST develops a cold tongue in boreal summer and is hardly distinguishable from observations in September–March. However, heat flux correction fails to completely eliminate the SST bias. This is evident in May–July, where the bias reaches a value of 1.19°C. The problem is that the model fails to produce the initial cooling in April–May that marks the onset of the observed cold tongue. Consequently, from April until August, FLX effectively lags behind the observed seasonal cycle by 1 month. The bias is 0.76°C on average from June to September and vanishes in boreal winter. Note that our SST bias reduction in boreal summer in ATL3 is comparable to the reduction that Harlaß *et al*. (2015) achieve by increasing the horizontal and vertical resolution of the KCM.

Regarding the monthly variability of the two initialization runs, Figure 2 shows the ACC between ERA-Interim and both STD and FLX for ATL3-SST. STD generally fails to produce the observed SST variability. A notable exception is boreal winter: STD is least biased then (Figure 1) and the

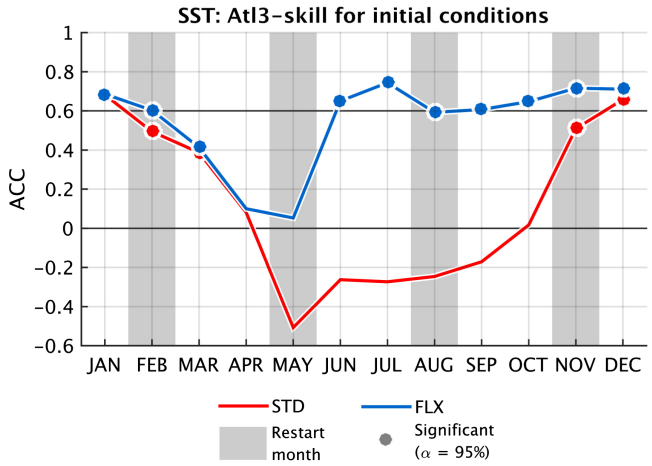

FIGURE 2 Monthly anomaly correlation coefficient (ACC) between ERA-Interim and the KCM initialization runs for the (blue) FLX and (red) STD experiments. ACC-values that are significantly different from 0 at the 95%-level according to a one-sided *t* test are shown as circles. Grey background bars show months during which seasonal hindcasts have been started from the initialization runs

prescribed wind stress forcing can interact with the model to produce roughly the observed variability. Compared to STD, FLX improves ACCs in boreal summer. This is encouraging, since it indicates that the FLX initialization run is able to capture the SST variability in boreal summer that is associated with the Atlantic Niño. A caveat is that FLX, too, is not able to reproduce the observed SST variability in April and May. We hypothesize that this feature is related to FLX's failure to produce the correct initial cooling during March–April.

3.2 | Skill of the seasonal hindcasting experiments

We present the skill of three distinct hindcasts:

1. The *anomaly persistence hindcast* is our reference. It is based on ERA-Interim SST. For each hindcast, we select reanalysis SST for lead month 0, that is, the month before the corresponding KCM hindcast has been started. We calculate the anomaly of ERA-Interim SST for lead month 0 relative to the linear fit and create a hindcast by persisting the anomaly throughout the hindcast period. In this way, our persistence hindcasts are comparable with our KCM hindcasts because their initial conditions do not use data that have been collected after the hindcast start. The skill of the persistence hindcasts is estimated via the ACC with ERA-Interim and is shown by the black line in Figure 3.
2. *Dynamical hindcasts* are the hindcasts produced by the two coupled model experiments. They are shown as light blue and light red lines in Figure 3 for the FLX and STD hindcasts, respectively.
3. Since SST evolves freely in the initialization runs, initial conditions for the dynamical hindcasts can differ from observed SST. To account for this error, we show the skill of *corrected hindcasts.* These hindcasts are based on the dynamical hindcasts, but add the difference between the initialization run and ERA-Interim SST at lead month 0 to each time step of the dynamical hindcast. This offline correction combines persistence and dynamical hindcasts. The information we use for the

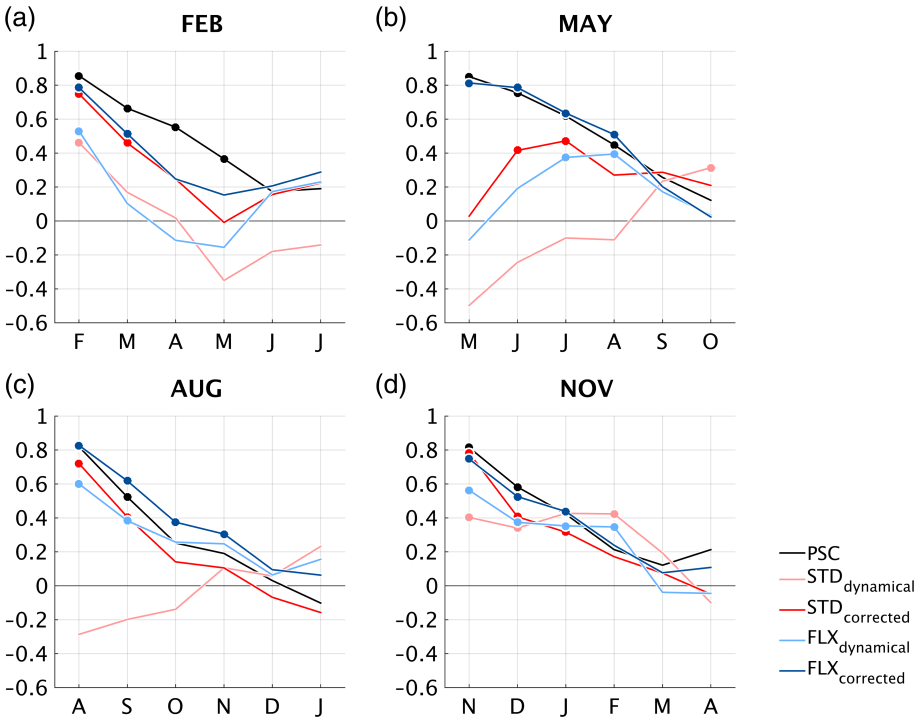

FIGURE 3 Hindcast skill (ACC) for SST in ATL3 for hindcasts initialized at the beginning of (a) February, (b) May, (c) August, (d) November. Circles show ACCs that are significantly different from 0 at the 95%-level. Line colours show the different experiments: (black) persistence, (light red) dynamical STD, (light blue) dynamical FLX, (red) corrected STD, (blue) corrected FLX hindcasts

correction is all known at the time of hindcast start, as for a real forecast. In Figure 3, the corrected hindcasts are shown as blue and red lines for the FLX and STD KCM hindcasts, respectively.

Figures 3a–d show the predictive skill of the hindcasts initialized at the beginning of February, May, August and November. Predictive skill for hindcasts started in February is not satisfactory (Figure 3a). All hindcasts lose skill quickly, and neither the dynamical nor the corrected hindcasts beat persistence. While corrected FLX hindcasts perform marginally better than corrected STD hindcasts, no clear improvement due to bias alleviation emerges from the dynamical hindcasts. The dynamical STD and FLX hindcasts achieve ACC values of about 0.44 and 0.53 for lead month 1 (February). These values, in the case of FLX, are not worse than for August or November hindcasts. However, skill drops quickly in February, implying that the February initial conditions contain little predictive potential.

May hindcasts perform differently in several aspects (Figure 3b). Overall, the corrected FLX May hindcasts achieve the best and most long-lived skill of our entire hindcasting experiment. The skill of the corrected FLX hindcasts is comparable to or slightly better than persistence for most of the hindcast. Skill drops more slowly than in February, and FLX experiments perform better than STD experiments. As indicated by Figure 2, skill for lead month 1 is very low for the (uncorrected) dynamical hindcasts. This is due to the failure of the partially coupled KCM, both in STD and FLX mode, to capture the observed SST variability. Both dynamical hindcasts, however, recover skill after a few months. Dynamical FLX hindcasts achieve ACCs that are significantly different from 0 at the 95% level based on a one-sided Student *t* test in July and August, STD in October. This, importantly, implies that the initial conditions contain information that can evolve into a predictable signal, despite the SST being unrealistic at the time of initialization. This information cannot reside in the SST field. Rather, we expect that subsurface processes such as thermocline displacement are responsible for the rise in hindcast skill over the course of the hindcast (see Section 4 for more discussion).

Dynamical FLX hindcasts start to perform better when started in August (Figure 3c). Notably, corrected FLX hindcasts also beat persistence when initialized in August, implying that dynamical hindcasting adds to the hindcast quality in August. As in May, while the initial conditions for the dynamical STD hindcasts are unrealistic due to the presence of the SST bias, even the STD experiment contains information that appears to raise the ACC throughout the hindcast, although the ACC values are never significant. This behaviour is encouraging, since it implies that the dynamical processes in both model versions are potentially able to capture aspects of observed SST variability.

Last, (uncorrected) dynamical hindcasts perform best in November (Figure 3d), although not better than persistence. The skill of the dynamical hindcasts is significantly different from 0 until lead month 4 for both FLX and STD. Notably, dynamical STD skill even beats dynamical FLX skill from lead month 2 onwards.

4 | SUMMARY AND DISCUSSION

In this paper, we have considered the impact of bias alleviation via a simple heat flux correction on the seasonal hindcast skill for equatorial Atlantic SST, and reported that bias alleviation generally improves hindcast skill. Additionally, we assessed the skill of reference persistence hindcasts, and corrected our KCM hindcasts with observed SSTs via an offline technique.

We identify a pronounced seasonality of the hindcast skill. Hindcasts generally perform badly when initialized at the start of February, despite starting from acceptable (SST) initial conditions. On the other hand, hindcasts initialized at the beginning of May exhibit the best performance among our experiments, despite unrealistic initial conditions for SST in both the standard (STD) and flux-corrected (FLX) dynamical hindcasts. Starting off with low SST skill, dynamical hindcasts recover skill throughout the hindcast, pointing to the existence of a predictable signal in the May initial conditions. Then, when correcting for the initial error in May SST, (corrected) dynamical hindcasts using the flux corrected model (FLX) achieve the best skill of all the hindcasts considered here.

To understand our results, we refer to Dippe *et al.* (2018a). These authors analysed the Bjerknes feedback in the ATL3 region in the partially coupled runs used to initialize our hindcasts, and compared the strength of this feedback to an estimate based on observations (see their Figure 10). The components of the Bjerknes feedback are the relationship between variations in (a) thermocline depth (using sea surface height [SSH] as a surrogate) and SST, (b) SST and the eastward wind component to the west of the ATL3 region, and (c) the same wind component and thermocline depth in the ATL3 region. In observations, the three components are at their strongest in late boreal spring and early summer forming a closed feedback loop that is missing in STD but is present to some extent in FLX, probably because of the improved thermocline structure in FLX (see Figure S1 in Ding *et al.* (2015)). This is why our FLX hindcasts beginning in May show the best performance. Additionally, the SSH–SST link becomes active at the end of the boreal summer in STD, when STD hindcasts initialized in May start to develop some (weak) skill. Despite the improvement in FLX compared to STD, the feedback loop is clearly much

stronger in observations than in FLX, suggesting that further model improvements can potentially lead to greater skill.

Stockdale *et al.* (2011) note the importance of reducing model error for successful prediction of equatorial Pacific SST through the so-called spring predictability barrier (e.g., Chen *et al.,* 1997; Latif *et al.,* 1998; Samelson and Tziperman, 2001; Duan and Wei, 2013). This barrier is illustrated by the relatively poor performance of our Pacific hindcasts, shown in Figure S3, that are initialized at the beginning of February. The similar behaviour we see in the Atlantic suggests that such a barrier could exist in the equatorial Atlantic (Figure 3a) as well.

Finally, since FLX uses a global heat flux correction, one might ask whether improved prediction in the Pacific contributes to our improved results in the Atlantic. However, Figure S3 indicates that this is unlikely, since there is little difference in the skill in the Pacific between STD and FLX.

To conclude, further work is clearly needed to reduce the tropical Atlantic warm bias in models. One possible route among others is to improve the atmospheric model — especially the vertical resolution, as pointed out by Harlaß *et al.* (2015; 2018).

ACKNOWLEDGEMENTS

We appreciate helpful comments from an anonymous reviewer. R.J.G. is grateful for continuing support from GEOMAR. The data used in this study can be obtained from GEOMAR's OPeNDAP Service at https://data.geomar.de.

CONFLICT OF INTEREST

The authors declare no potential conflict of interest.

REFERENCES

Bell, M.J., Martin, M.J. and Nichols, N.K. (2004) Assimilation of data into an ocean model with systematic errors near the equator. *Quarterly Journal of the Royal Meteorological Society*, 130, 873–893.

Bjerknes, J. (1969) Atmospheric teleconnections from the equatorial Pacific. *Monthly Weather Review*, 97, 163–172.

Burls, N.J., Reason, C.J.C., Penven, P. and Philander, S.G. (2011) Similarities between the tropical Atlantic seasonal cycle and ENSO: an energetics perspective. *Journal of Geophysical Research: Oceans*, 116, C11010.

Burls, N.J., Reason, C.J.C., Penven, P. and Philander, S.G. (2012) Energetics of the tropical Atlantic zonal mode. *Journal of Climate*, 25, 7442–7466.

Chen, D., Zebiak, S.S.E., Cane, M.A. and Busalacchi, A.J. (1997) Initialization and predictability of a coupled ENSO forecast model. *Monthly Weather Review*, 125, 773–788.

Davey, M., Huddleston, M., Sperber, K., Braconnot, P., Bryan, F., Chen, D., Colman, R., Cooper, C., Cubasch, U., Delecluse, P., DeWitt, D., Fairhead, L., Flato, G., Gordon, C., Hogan, T., Ji, M., Kimoto, M., Kitoh, A., Knutson, T., Latif, M., Le Treut, H., Li, T., Manabe, S., Mechoso, C., Meehl, G., Power, S., Roeckner, E., Terray, L., Vintzileos, A., Voss, R., Wang, B., Washington, W., Yoshikawa, I., Yu, J., Yukimoto, S. and Zebiak, S. (2002) STOIC: a study of coupled model climatology and variability in tropical ocean regions. *Climate Dynamics*, 18, 403–420.

Dee, D.P., Uppala, S.M., Simmons, A.J., Berrisford, P., Poli, P., Kobayashi, S., Andrae, U., Balmaseda, M.A., Balsamo, G., Bauer, P., Bechtold, P., Beljaars, A.C.M., van de Berg, L., Bidlot, J., Bormann, N., Delsol, C., Dragani, R., Fuentes, M., Geer, A.J., Haimberger, L., Healy, S.B., Hersbach, H., Hólm, E.V., Isaksen, L., Kållberg, P., Köhler, M., Matricardi, M., Mcnally, A. P., Monge-Sanz, B.M., Morcrette, J.J., Park, B.K., Peubey, C., de Rosnay, P., Tavolato, C., Thépaut, J.-N. and Vitart, F. (2011) The ERA-Interim reanalysis: configuration and performance of the data assimilation system. *Quarterly Journal of the Royal Meteorological Society*, 137, 553–597.

Ding, H., Keenlyside, N.S. and Latif, M. (2009) Seasonal cycle in the upper equatorial Atlantic Ocean. *Journal of Geophysical Research: Oceans*, 114, C09016.

Ding, H., Greatbatch, R.J., Latif, M., Park, W. and Gerdes, R. (2013) Hindcast of the 1976/77 and 1998/99 climate shifts in the Pacific. *Journal of Climate*, 26, 7650–7661.

Ding, H., Greatbatch, R.J., Latif, M. and Park, W. (2015) The impact of sea surface temperature bias on equatorial Atlantic interannual variability in partially coupled model experiments. *Geophysical Research Letters*, 42, 5540–5546.

Dippe, T., Greatbatch, R.J. and Ding, H. (2018a) On the relationship between Atlantic Niño variability and ocean dynamics. *Climate Dynamics*, 51, 597–612.

Dippe, T., Krebs, M., Harlaß, J. and Lübbecke, J.F. (2018b) Can climate models simulate the observed strong summer surface cooling in the equatorial Atlantic? In: *YOUMARES 8 – Oceans Across Boundaries: Learning from Each Other*. Springer, pp. 7–23.

Dippe, T., Lübbecke, J.F. and Greatbatch, R.J. (2019) A comparison of the Atlantic and Pacific Bjerknes feedbacks: seasonality, symmetry, and stationarity. *Journal of Geophysical Research: Oceans*. https://doi.org/10.1029/2018JC014700.

Duan, W. and Wei, C. (2013) The 'spring predictability barrier' for ENSO predictions and its possible mechanism: results from a fully coupled model. *International Journal of Climatology*, 33, 1280–1292.

Grodsky, S.A., Carton, J.A., Nigam, S. and Okumura, Y.M. (2012) Tropical Atlantic biases in CCSM4. *Journal of Climate*, 25, 3684–3701.

Harlaß, J., Latif, M. and Park, W. (2015) Improving climate model simulation of tropical Atlantic sea surface temperature: the importance of enhanced vertical atmosphere model resolution. *Geophysical Research Letters*, 42, 2401–2408.

Harlaß, J., Latif, M. and Park, W. (2018) Alleviating tropical Atlantic sector biases in the Kiel climate model by enhancing horizontal and vertical atmosphere model resolution: climatology and interannual variability. *Climate Dynamics*, 50, 2605–2635.

Hirst, A.C. and Hastenrath, S. (1983) Atmosphere–ocean mechanisms of climate anomalies in the Angola-tropical Atlantic sector. *Journal of Physical Oceanography*, 13, 1146–1157.

Keenlyside, N.S. and Latif, M. (2007) Understanding equatorial Atlantic interannual variability. *Journal of Climate*, 20, 131–142.

Latif, M., Anderson, D. and Barnett, T. (1998) A review of the predictability and prediction of ENSO. *Journal of Geophysical Research: Oceans*, 103, 14375–14393.

Lübbecke, J.F. and McPhaden, M.J. (2013) A comparative stability analysis of Atlantic and Pacific Niño modes. *Journal of Climate*, 26, 5965–5980.

Madec, G. (2008) *NEMO ocean general circulation model reference manual.* Tech. rep. Paris: Institut Pierre-Simon Laplace.

Madec, G., Delecluse, P., Imbard, M. and Levy, C. (1998) *OPA 8.1 general circulation model reference manual.* Tech. rep. Paris: Institut Pierre-Simon Laplace.

Mohino, E. and Losada, T. (2015) Impacts of the Atlantic equatorial mode in a warmer climate. *Climate Dynamics*, 45, 2255–2271.

Park, W., Keenlyside, N., Latif, M., Ströh, A., Redler, R., Roeckner, E. and Madec, G. (2009) Tropical Pacific climate and its response to global warming in the Kiel climate model. *Journal of Climate*, 22, 71–92.

Richter, I. and Xie, S.-P. (2008) On the origin of equatorial Atlantic biases in coupled general circulation models. *Climate Dynamics*, 31, 587–598.

Roeckner, E., Bäuml, G., Bonaventura, L., Brokopf, R., Esch, M., Giorgetta, M., Hagemann, S., Kirchner, I., Kornblueh, L., Rhodin, A., Schlese, U., Schulzweida, U. and Tompkins, A. (2003) *The atmospheric general circulation model ECHAM5: part 1: model description.* MPI report number: 1-140.

Samelson, R. and Tziperman, E. (2001) Instability of the chaotic ENSO: the growth-phase predictability barrier. *Journal of the Atmospheric Sciences*, 58, 3613–3625.

Scaife, A.A., Ferranti, L., Alves, O., Athanasiadis, P., Baehr, J., Dequé, M., Dippe, T., Dunstone, N., Fereday, D., Gudgel, R.G., Greatbatch, R.J., Hermanson, L., Imada, Y., Jain, S., Kumar, A., MacLachlan, C., Merryfield, W., Müller, W.A., Ren, H.-L., Smith, D., Takaya, Y., Vecchi, G. and Yang, X. (2019) Tropical rainfall predictions from multiple seasonal forecast systems. *International Journal of Climatology*, 39, 974–988.

Stockdale, T.N., Balmaseda, M.A. and Vidard, A. (2006) Tropical Atlantic SST prediction with coupled ocean–atmosphere gcms. *Journal of Climate*, 19, 6047–6061.

Stockdale, T.N., Anderson, D.L., Balmaseda, M.A., Doblas-Reyes, F., Ferranti, L., Mogensen, K., Palmer, T.N., Molteni, F. and Vitart, F. (2011) ECMWF seasonal forecast system 3 and its prediction of sea surface temperature. *Climate Dynamics*, 37, 455–471.

Thoma, M., Greatbatch, R.J., Kadow, C. and Gerdes, R. (2015) Decadal hindcasts initialized using observed surface wind stress: evaluation and prediction out to 2024. *Geophysical Research Letters*, 42, 6454–6461.

Valcke, S. (2013) The OASIS3 coupler: a European climate modelling community software. *Geoscientific Model Development Discussions*, 5, 2139–2178.

Wang, C., Zhang, L., Lee, S., Wu, L. and Mechoso, C.R. (2014) A global perspective on CMIP5 climate model biases. *Nature Climate Change*, 4, 201–205.

Xie, S.-P. and Carton, J.A. (2004) Tropical Atlantic variability: Patterns, mechanisms, and impacts. In: Earth Climate: The Ocean-Atmosphere Interaction. *Geophysical Monograph*, 147, 121–142. https://doi.org/10.1029/GM147.

Zebiak, S.E. (1993) Air–sea interaction in the equatorial Atlantic region. *Journal of Climate*, 6, 1567–1586.

SUPPORTING INFORMATION

Additional supporting information may be found online in the Supporting Information section at the end of this article.

How to cite this article: Dippe T, Greatbatch RJ, Ding H. Seasonal prediction of equatorial Atlantic sea surface temperature using simple initialization and bias correction techniques. *Atmos Sci Lett*. 2019;20: e898. https://doi.org/10.1002/asl.898